CFD SIMULATION OF GAS-LIQUID HYDRODYNAMICS IN AERATED STIRRED TANK

AZRI ABDULLAH

A thesis submitted in fulfillment of

the requirement of the award of the degree of

Bachelor of Chemical Engineering

Faculty of Chemical and Natural Resources Engineering

University Malaysia Pahang

APRIL 2010

ABSTRACT

The aim of this work is to comparing the simulation result from Computational Fluid Dynamic (CFD) with the experimental measurement from Montante *et al.* (2007). Liquid axial velocity and liquid radial velocity were measured in order to get the similar result with experimental measurement from Montante *et al.* (2007). For this work, Gambit 2.4.6 and Fluent 6.3.26 software were use in modelling and running the simulation. The experimental results obtained at different gas flow rates are presented, compared with multi-phase data and discussed for gaining insight into the gas–liquid flows. The agreement between the experimental and the calculated mean velocity fields indicates that the selected CFD modelling is appropriate for the prediction of the mean hydrodynamic features of gas–liquid dispersions in stirred vessels.

ABSTRAK

Tujuan kerja ini adalah untuk membandingkan keputusan simulasi dari Pengkomputeran Cecair Dynamic (CFD) dengan hasil pengukuran eksperimental dari Montante *et al*. (2007). Cecair kelajuan axial dan kelajuan jejari cecair diukur untuk mendapatkan keputusan yang serupa dengan pengukuran eksperimental dari Montante *et al*. (2007). Untuk penghasilan ini, perisian Gambit 2.4.6 dan Fluent 6.3.26 digunakan dalam pemodelan dan menjalankan simulasi. Keputusan eksperimen diperolehi pada kelajuan aliran gas berbeza dibentangkan, berbanding dengan data multi-fasa dan dibincangkan untuk mendapatkan pandangan tentang aliran gas-cecair. Perjanjian antara eksperimental dan pengiraan bidang min kelajuan menunjukkan bahawa pemodelan CFD yang dipilih sesuai untuk ramalan ciri min hidrodinamika dispersi gas cecair di dalam tangki pembancuhan.

TABLE OF CONTENTS

CHAPTER	TITLE	PAGE
	DECLARATION OF ORIGINAL WORK	i
	DEDICATION	ii
	ACKNOWLEDGEMENTS	iii
	ABSTRACT	iv
	ABSTRAK	v
	TABLE OF CONTENTS	vi
	LIST OF FIGURES	viii
	LIST OF ABBREVIATIONS	x
1	**INTRODUCTION**	
	1.1 Motivation	1
	1.2 Research Objective	2
	1.3 Scope of Study	3
2	**LITERATURE REVIEW**	
	2.1 Design of Aerated Stirred Tanks	4
	2.2 Impellers in Mixing Tanks	4
	2.3 Gas-Liquid Hydrodynamics	5
	2.4 Computational Fluid Dynamics (CFD)	6
	2.5 Turbulence	6
	2.6 Gas-Liquid Mixing	7
	2.6.1 Surface Aeration Phenomena in Stirred Tank	7
	2.6.2 Aerated Impeller Power Consumption and Gas Flow Patterns	9
	2.6.3 Gas Voidage Fraction and Interfacial	14

3	**MATHEMATICAL MODELLING**	
	3.1 Overview	17
	3.2 Introduction	17
	3.2.1 Gas-Liquid Stirred Vessel modeling	17
	3.2.2 CFD Modelling of Two-Phase Flow	19
	3.3 Turbulence Modelling	20
	3.4 CFD approach for aerated stirred tank	21
	3.5 Step for CFD modelling	23
	3.6 Summary	26
4	**RESULT AND DISCUSSION**	
	4.1 Overview	27
	4.2 Result and Discussion	27
	4.3 Summary	36
5	**CONCLUSION AND RECOMMENDATION**	
	5.1 Conclusion	37
	5.2 Recommendation	37
	REFERENCES	38
	APPENDICES	
	APPENDIX A	40
	APPENDIX B	42

LIST OF FIGURES

FIGURE NO.	TITLE	PAGE
2.1	Force / free vortex rotation in an unbaffled tank	8
2.2	Surface entrainment mechanism in baffled tanks	8
2.3	Gassed power ratio for a standard disk turbine	10
2.4	Cavity shapes formed on blades during gas-liquid dispersion	11
2.5	Gas flow map for standard disk turbine, showing regions of different cavity formation	12
2.6	Gas flow patterns as a function of impeller speed and gas flow rate	13
3.1	Aerated stirred tank geometry	24
4.1	R=0.29T axial velocity (CFD result)	27
4.2	R=0.48T axial velocity (CFD result)	28
4.3	Experimental measurement from Montante et.al (2007): (solid triangle line; r=0.29T: solid bubble line; 0.48T).	28
4.4	Comparison of liquid axial velocity between experimental measurement from Montante et al 2007 and experimental measurement from CFD for 0.29T	29
4.5	Comparison of liquid axial velocity between experimental measurement from Montante et.al 2007 and experimental measurement from CFD for 0.48T	29
4.6	R=0.45T axial velocity (CFD result)	30
4.7	Experimental measurement from Montante et.al. 2007 (rectangle line)	31

4.8	Comparison of gas flow rate on the liquid axial velocity between experimental measurement from Montante et al 2007 and experimental measurement from CFD for 0.45T	31
4.9	R=0.46T axial velocity (CFD result)	32
4.10	Experimental measurement from Montante et al 2007 (solid thin line)	33
4.11	Comparison of liquid axial velocity between experimental measurement from Montante et al 2007 and experimental measurement from CFD for 0.46T	33
4.12	R=0.46T radial velocity (CFD result)	34
4.13	Experimental measurement from Montante et al 2007 (solid thin line)	35
4.14	Comparison of liquid radial velocity between experimental measurement from Montante et al 2007 and experimental measurement from CFD for 0.46T	35

LIST OF ABBREVIATIONS

SYMBOL	DEFINITION	UNIT
a	Area of bubble	m^2
C	Impeller clearance	m
C_D	Bubble drag ceofficient	dimensionless
C_{vm}	Constant	dimensionless
D	Impeller diameter	m
d_b	Bubble diameter	m
d_{10}	bubble number (arithmetic mean) diameter	m
d_{32}	volume-to-surface (Sauter) diameter	m
d_{43}	weight mean diameter	m
F_D	Drag force	N
F_{vm}	Virtual mass force	N
$\vec{F}_{lg}$	Interaction force mainly due to drag	N
g	Gravity acceleration	ms^{-2}
H	Vessel height	m
k	turbulent kinetic energy	m^2s^{-2}
M_{IK}	Momentum transfer forces	N
N	Agitation speed	s^{-1}
Re_b	bubble Reynolds number	dimensionless
U	mean axial velocity	ms^{-2}
u_t	turbulent velocity	ms^{-2}
Q_G	Gas flow rate	vvm
V	mean radial velocity	ms^{-2}
v_b	volume of bubble	m^3
V_{tip}	impeller tip speed	ms^{-2}
z	axial coordinate	m

CHAPTER 1

INTRODUCTION

1.1 Motivation

Stirred vessels are widely used in chemical, pharmaceutical, food and metallurgical process industries as well in municipal and industrial wastewater treatment. In these processes, the requirement of quality of mixing varies over a wide range. These include blending of low viscosity of liquids, high viscosity liquids or high viscosity liquids with low viscosity liquids and vice versa, solid-solid mixing, etc. These also include heat transfer and large number of dispersion applications such as gas–liquid. The quality of mixing mainly depends upon the relative distribution of mean and turbulent kinetic energy. One extreme is the absence of turbulence and the entire energy exists in the form of mean kinetic energy. The other extreme is that the flow is turbulent at all the locations and the mean velocities are zero. Obviously, the real flow is in between the two extremes and depends upon impeller design, diameter and the location of impellers, vessel diameter, bottom design and internals such as coils, baffles, draft tube, etc. The desired flow pattern (relative distribution of mean and turbulent kinetic energy) depends upon the application. For instance, blending application prefers all the energy in the form of mean and minimal turbulent kinetic energy. On contrast, colloidal mills, homogenizers and emulsifiers need highly turbulent flows. All the other applications can be conveniently classified according to their need of energy distribution.

According to J.Gimbun *et al*, it is hard to find single measurement techniques that could provide all information on the gas-liquid stirred tanks. For instance,

gamma-ray and x-ray tomography is an excellent method for measuring the gas holdup distribution, but it does not give an information regarding the two-phased flow field and bubble size and this equipment are too expensive. Similarly, the computed-automated radioactive particle tracking (CARPT) is capable of measuring the two-phased flow field at high gas loading, but it cannot be applied to measure bubble size distribution and gas holdup.

In stirred vessels, the quality of flow generated by the impeller mainly depends upon the impeller design. Typically, low power number impellers generate mean flow whereas high power number impeller generate flow having more turbulent kinetic energy. As the flow proceeds from the impeller and circulates within the vessel, the mean kinetic energy is converted into turbulent kinetic energy and as mentioned earlier, the relative distribution at any location depends upon the design of the impeller, vessel and internals. In view of such an immense importance of the knowledge of quality of flow, vigorous research efforts have been made during the last 50 years using various flow measurement techniques and computational fluid dynamics (CFD) which can provide all information and description about gas-liquid hydrodynamics. A brief review has been presented below for getting a flavour of the existing status of knowledge.

1.2 Research Objective

To study effect of impeller blade to axial and radial liquid velocity behavior of gas-liquid flow in aerated stirred tank and compare with experimental values from past research

1.3 Scope of Study

To develop a modelling method for hydrodynamics and gas dispersion in single phase and aerated stirred tanks with the intension of elucidating design and scale up methods for gas-liquid stirred tanks via CFD (Computational Fluid Dynamics)

CHAPTER 2

LITERATURE REVIEW

2.1 Design of Aerated Stirred Tanks

Most aerated stirred tanks are designed to achieved high mass transfer rate. Interfacial area is well known as a major indicator of mass transfer performance in an aerated system and thus it becomes a primary concern in aerated stirred tank design. (Tatterson 1994)

The function of the agitation system is to provide good mixing and thus increase mass transfer rates through the bulk liquid and bubble boundary layers, to provide the appropriate shear conditions required for the breaking up of bubbles, the agitation system consists of the agitator and the baffles and the baffles are used to break the liquid flow to increase turbulence and mixing efficiency.

2.2 Impellers in Mixing Tanks

Impellers in agitated tanks are used to mix fluids or slurry in the tank. This can be used to combine materials; solids, liquids, gas. Mixing the fluids in a tank is very important if there are gradients in conditions such as temperature or concentration.

There are two types of impellers, depending on the flow regime created: axial flow impeller and radial flow impeller.

Radial flow impellers impose essentially shear stress to the fluid, and are used, for example, when we need to mix immiscible liquids or in general when there is a deformable interface to break. Another application of radial flow impellers are the mixing of very viscous fluids.

Axial flow impellers impose essentially bulk motion, and are used on homogenization processes, in which is important to increase fluid volumetric flow rate.

2.3 Gas-Liquid Hydrodynamics

A three phase fluidized bed reactor provides contact between gas and liquid phases, and solid particles. Currently, almost all the major oil companies in United States operate at least a hydrotreating/hydrogenation reactor in which long chain residual oil molecules are catalytically converted to gasoline or jet fuel grade saturated hydrocarbons by hydrogen substitution.

There are also numerous applications of gas-liquid (i.e. bubble column), liquid-solid, and/or gas-liquid-solid fluidization in biological and pharmaceutical processes. In general, fluidized beds when compared to fixed bed operations provide lower pressure, higher heat and mass transfer rates, better mixing and ease of operation with respect to handling of solid phase. The main drawbacks of the fluidized beds are their non-ideal CSTR behaviour which results in lower conversion rate for catalytic reactions and complicated operations.

2.4 Computational Fluid Dynamic (CFD)

Computational fluid dynamics, or CFD, is the numerical simulation of fluid motion. While the motion of fluids in mixing is an obvious application of CFD, there are hundreds of others, ranging from blood flow through arteries, to supersonic flow over an airfoil, to the extrusion of rubber in the manufacture of automotive parts. Numerous models and solution techniques have been developed over the years to help describe a wide variety of fluid motion.

2.5 Turbulence

A number of dimensionless parameters have been developed for the study of fluid dynamics that are used to categorize different flow regimes. These parameters, or numbers, are used to classify fluids as well as flow characteristics. One of the most common of these is the Reynolds number, defined as the ratio of inertial forces, or those that give rise to motion of the fluid, to frictional forces, or those that tend to slow the fluid down. In geometrically similar domains, two fluids with the same Reynolds number should behave in the same manner. For simple pipe flow, the Reynolds number is defined as

$$Re = \frac{\rho U d}{\mu} \qquad 2.1$$

where ρ is the fluid density, U is the axial velocity in the pipe, d is the pipe diameter, and μ is the molecular, or dynamic viscosity of the fluid. For mixing tanks, a modified definition is used:

$$Re = \frac{ND^2\rho}{\mu} \qquad 2.2$$

where N is the impeller speed, in revolutions/sec, and D is the impeller diameter. Based on the value of the Reynolds number, flows fall into either the laminar regime,

with small Reynolds numbers, or the turbulent regime, with high Reynolds numbers. The transition between laminar and turbulent regimes occurs throughout a range of Reynolds numbers, rather than at a single value. For pipe flow, transition occurs in the vicinity of Re = 2000, while in mixing tanks, it is usually different, occurring somewhere between Re = 50 and 5000. In the turbulent regime, fluctuations in the mean velocity and other variables occur, and their effect needs to be incorporated into the CFD model in order for the model to be able to provide meaningful results. This is done through the use of a turbulence model.

Several methods are available for including turbulence in the Navier-Stokes equations. Most of these involve a process of time-averaging the conservation equations. When turbulence is included, the transported quantity, say velocity, is assumed to be the sum of an equilibrium and a fluctuating component, Ui + ui.

2.6 Gas-Liquid Mixing

2.6.1 Surface Aeration Phenomena in Stirred Tank

In many food processing applications it is important to avoid entraining air during the mixing process, since this causes spoilage during product storage. Many workers have noted that in the absence of gas sparging, surface aeration occurs above a minimum impeller speed denoted by NSA. The forced / free vortex model illustrated in Figure 2.1 for flow in an unbaffled tank may be used to predict the point at which the free surface reaches the impeller (typically, for a Rushton turbine the change from forced to free vortex flow occurs at a radius of 3D / 8). (Greaves & Kobbacy, 1981) gave a qualitative description of the aeration phenomena from the free surface in baffled tanks, at N > NSA. Strong eddies (A in Figure. 2.2), formed by the interaction of the discharge flow from the impeller with the baffles, induce other strong eddies (B in Figure 2.2) which process slowly around the impeller shaft and form a hollow vortex at the surface.

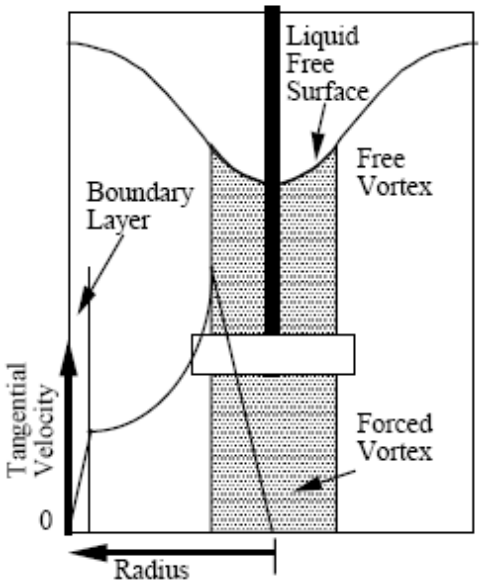

Figure 2.1: Force / free vortex rotation in an unbaffled tank

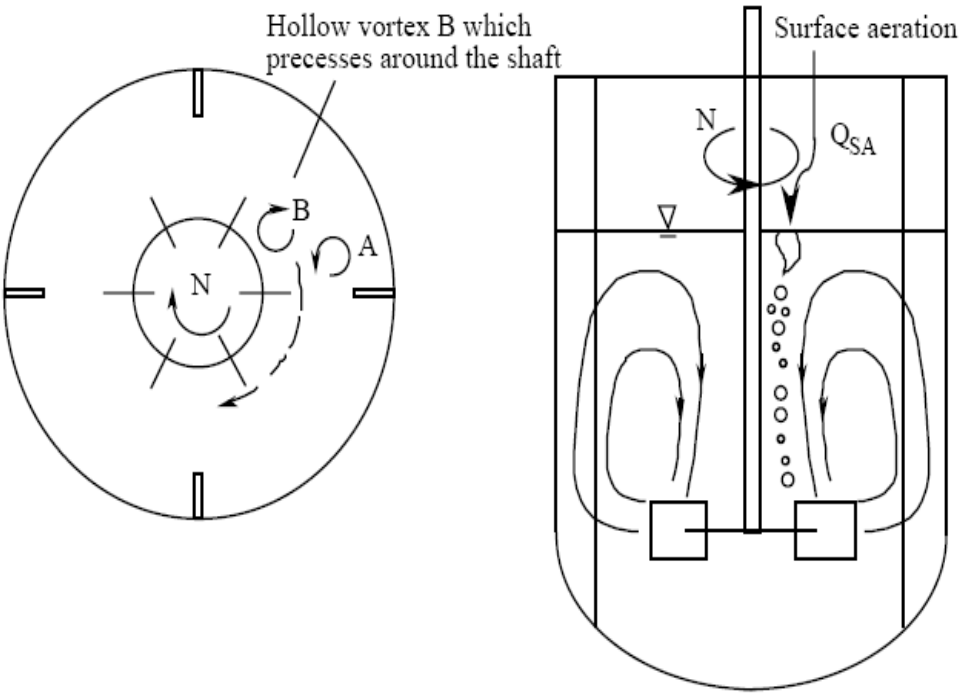

Figure 2.2: Surface entrainment mechanism in baffled tanks.

(Van Dierendonck *et al*, 1968) and Joshi *et al.* (1982) have correlated NSA, the critical speed for the onset of aeration against physical properties and geometric parameters. Van Dierendonck's correlation for a standard disc turbine in a baffled tank is

$$\left(\frac{\rho_L N_{SA} D^2}{T\sigma}\right)\left(\frac{\rho L\sigma^3}{g\mu^4 L}\right)^{\frac{1}{4}} = 2.0\left(\frac{H-C}{C}\right)^{\frac{1}{2}}\left(\frac{1}{2}\right) \qquad 2.3$$

Which is restricted to

$$0.10 \leq \frac{H-C}{T} \leq 0.20 + 1.75\frac{D}{T} \qquad 2.4$$

2.6.2 Aerated Impeller Power Consumption and Gas Flow Patterns

The effect of sparging gas bubbles into a stirred tank is to substantially reduce the power consumption of the impeller. In gas-liquid applications the gassed power input is fairly high (1 - 2 kW / m^3) since large energy dissipation rates produce small bubbles and large interfacial areas. Uhl & Gray (Vol. I, pp.145–148, 1966), Nagata (Chapter 8, 1975) and Greaves & Barigou (1986) have reviewed the literature on power consumption under aerated conditions. The best known correlation is by Michel & Miller (1962).

$$\frac{P_g}{} = C\left(\frac{P_o^2 N D^3}{Q_g^{0.56}}\right)^{0.45} \qquad 2.5$$

where C is a constant with values between 0.63 and 1.19, depending on tank diameter and geometry (all units are in SI). Mann (1983) gives C=0.72, but notes that equation 2.5 fails as the gas volumetric flow rate, therefore caution should be exercised in using this method for scale-up.

More recently workers have expressed their results in dimensionless terms by plotting the gassed power ratio P_g / P_o (taking values in the range 0 to 1) against the aeration number NQ = Q / ND3, at constant impeller speed, as shown in Figure 2.3. This figure is for a standard geometry disc turbine, but data is available in the literature for many other impeller designs. Since the power input partly determines rates of mass transfer in gas-liquid dispersions it is important that the gassed power number does not drop off too rapidly, as the aeration number increases. The Rushton turbine was formerly regarded as an efficient gas disperser, however it has a large ungassed power number and the power decreases by as much as 60% on aeration. Modern developments in gas-liquid agitator design have concentrated on impellers which maintain a value of Pg / Po close to unity over the operating range of aeration numbers

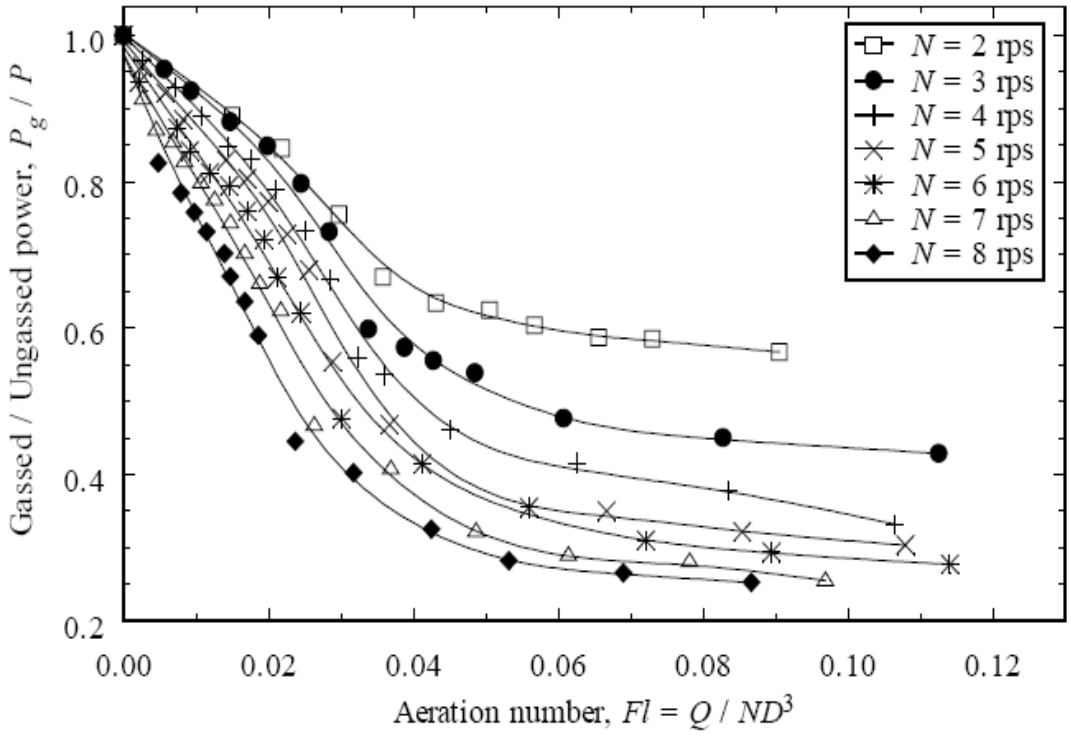

Figure 2.3: Gassed power ratio for a standard disk turbine
[van't Riet & Smith, 1978)]

Bruijn, van't Riet & Smith (1974) and van't Riet & Smith (1973) explained the decrease in gassed power consumption as a consequence of the formation of stable "gas cavities" behind the blades. Gas sparged into the vessel is trapped in vortices

trailing behind each impeller blade and may remain there for several revolutions before being dispersed as small bubbles in the highly turbulent wake of each cavity. For a continuous flow of gas, at a sufficiently high impeller speed, stable gas cavities form behind each blade; the size and shape of these cavities depends on gas volumetric flow rate and impeller speed, as illustrated by Figure 2.4. At low gas flow rates the bubbles are trapped in the trailing vortex system behind each blade and form so-called vortex cavities. As the sparged gas flow rate is increased the attached cavity size increases forming clinging and then large cavities. Smith (1986) has published flow regime maps (*e.g.* Figure 2.5) showing these cavity types as a function of the Froude and the aeration numbers. For NQ > ~0.06 the cavities form themselves into a three-three configuration for six-bladed impellers, *i.e.* there are large and small cavities on alternate blades. For five-bladed impellers the three-three configuration tries to form, but the odd large or small cavity precesses from blade to blade. The size of the attached cavity determines the drag coefficient for the blade, and thus the precessing cavity causes a fluctuating load on the blade and an imbalance of the forces acting on the shaft. It was quite common for the shafts of five-bladed impellers to break in gas-liquid operation and their use is avoided today.

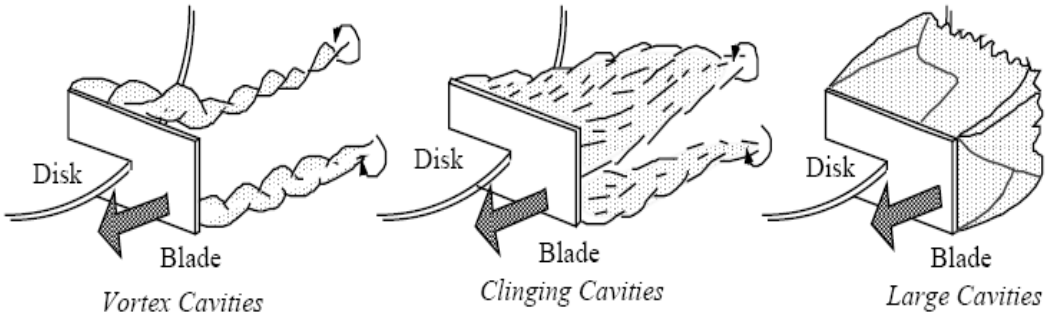

Figure 2.4: Cavity shapes formed on blades during gas-liquid dispersion.

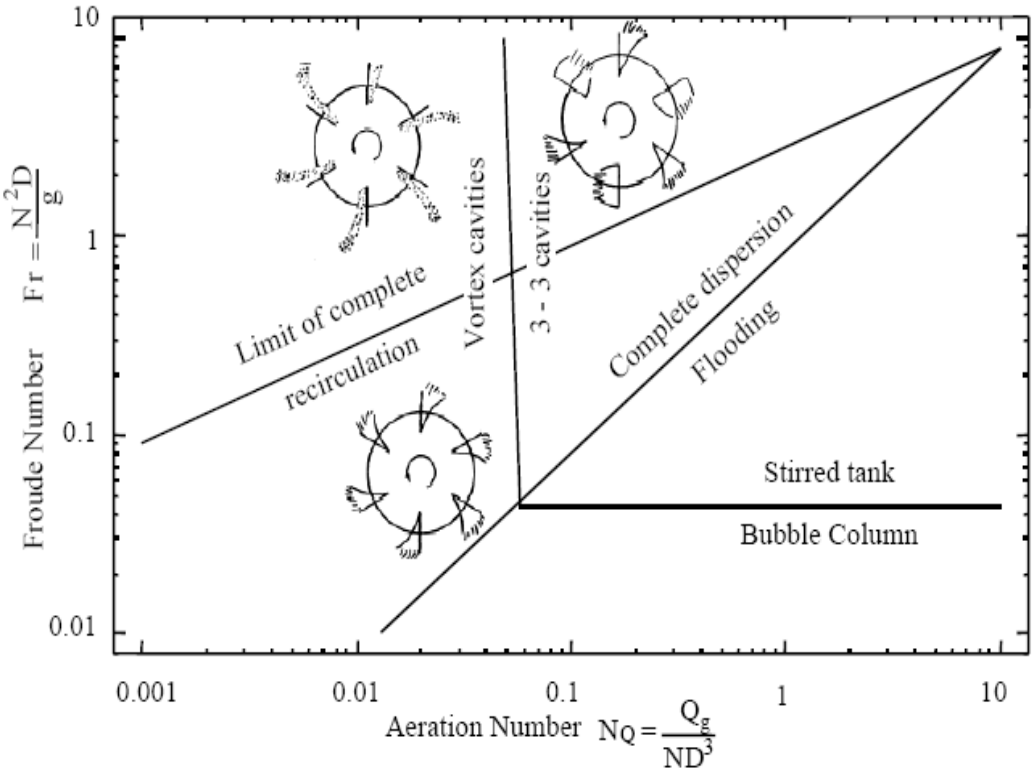

Figure 2.5: Gas flow map for standard disk turbine, showing regions of different cavity formation.

The presence of these cavities alters the liquid streamlines around the blade, such that the separation point occurs further downstream from the leading edge of the blade. Form drag on the impeller is decreased since the wake volume behind each blade is reduced by the presence of the gas cavity. Consequently, there is a reduction in power consumption in the presence of gas, which depends on the size and shape of the gas cavities.

Figure 2.6 demonstrates the effect of gradually increasing the gas throughput or decreasing the impeller speed on gas flow patterns in a gas-liquid stirred tank (Nienow *et al.*, 1978).

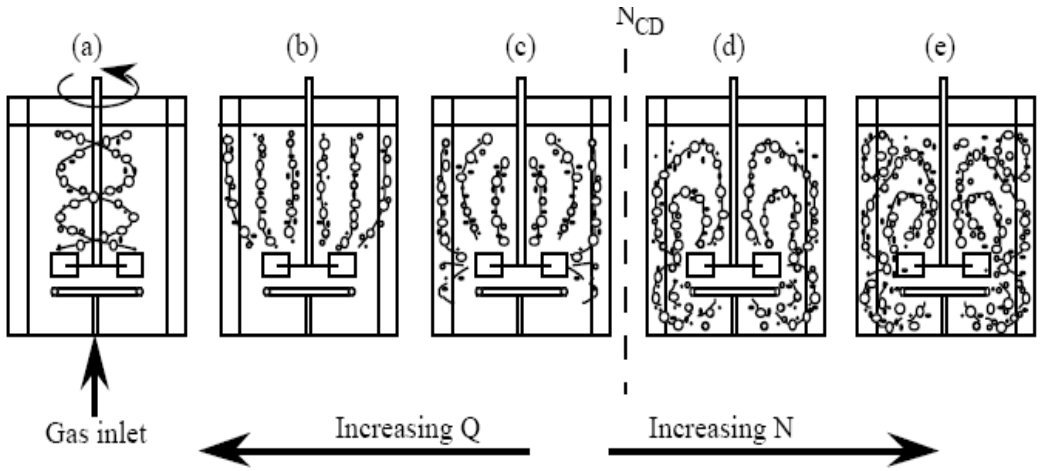

Figure 2.6: Gas flow patterns as a function of impeller speed and gas flow rate

At low gas flow rates and high impeller speeds the bubbles are well dispersed above and below the impeller; with increasing gas flow, the gas dispersion becomes worse. Nienow *et al.* (1978) defined a critical speed for complete dispersion, NCD, at the change from conditions (c) to (d) in Figure 2.6. For H = T, C = T / 4, 6-bladed disc turbines (valid for T < 1.8 m), Nienow *et al* 1978 correlated their results by

Pipe spargers: $$N_{CD} = 4\frac{Q^{0.5}T^{0.25}}{D^2}$$ 2.6

Ring spargers: $$N_{CD} = 3\frac{Q^{0.5}T^{0.25}}{D^2}$$ 2.7

Here Q is the volumetric flow rate of gas and all quantities are in SI units. These equations predict conservative values of N_{CD} for non-coalescing systems and turbines with more than six blades (Middleton, 1985).

Figure 2.3 shows that at constant impeller speed, the gassed power ratio becomes fairly constant at large values of aeration number, N_Q. Under these conditions the cavities have grown to their maximum size; further increasing the gas throughput leads to "flooding", corresponding to (a) in Figure 2.6. In the flooded condition, not all of the gas passes through the gas cavities and some is not dispersed by the impeller. At this point the impeller virtually stops pumping in the radial direction, and a bulk liquid circulation is set up by the rising bubbles

(Warmoeskerken & Smith, 1984). These workers showed theoretically that at the flooding point.

$$\frac{Q}{N_F D^3} = 1.2\frac{N_F^2 D}{g} \qquad 2.8$$

where NF is the critical impeller speed for flooding at a given gas volumetric flow rate, Q. Clearly, flooding is an undesirable condition, which should be avoided in practice since liquid phase mixing, gas dispersion and gas-liquid mass transfer are all adversely affected.

In many gas-liquid operations the process objective is to maintain the same level of power input at different gas inputs, *i.e.* to have a gassed power curve which is relatively flat, without much reduction in the ratio Pg / Po. This ensures that bubble sizes and mass transfer coefficients are not impaired. Recent developments in impeller design have shown that large numbers of blades (12 or 18) or concave blades give this type of behaviour (Middleton, 1985).

2.6.3 Gas Voidage Fraction and Interfacial Area in Stirred Tanks

In designing gas-liquid reactors or fermenters it is necessary to know the gas volume fraction held up in the liquid, so that the overall volume of the vessel may be calculated. The mean gas voidage fraction, ε , is defined as

$$\varepsilon = \frac{\mathbf{V_G}}{\mathbf{V_G} + \mathbf{V_L}} \qquad 2.9$$

where VG and VL are the gas and liquid volumes in the stirred tank, respectively. A large number of purely empirical correlations have been proposed for the gas voidage fraction in terms of the gas flow rate and impeller speed. Calderbank (1958) presented a semitheoretical method for predicting the mean gas voidage fraction; the method is based Kolmogoroff's theory of local isotropic turbulence, which is valid only at high Reynolds numbers. The analysis shows that the largest bubble size that

can exist in a given turbulent flow depends on the power input per unit volume, (P_g / V), the fluid density, ρ_L, and the surface tension,σ:

$$d_{max} \propto \sigma^0 . \frac{6}{\rho_L^0 . 2 \left(P_g/V\right)^0 . 4} \qquad 2.10$$

Calderbank correlated the Sauter mean bubble diameter, d_{32}, (a surface area, volume mean) data from stirred tank experiments using the expression.

$$d_{32} = 4.15 \left[\sigma^0 . \frac{6}{\rho_L^0 . 2 \left(P_g/V\right)^0 . 4}\right] \varepsilon^{0.5} + 9 \infty 10^{-4} \text{ meters} \qquad 2.11$$

Using similar arguments Calderbank also proposed that the interfacial area per unit volume was given by

$$a = 1.44 \left[\frac{\rho_L^0 . 2 \left(P_g/V\right)^0 . 4}{\sigma^0} . 6\right] \left[\frac{U_g}{V}\right]^0 . 5 \qquad 2.12$$

Here, Ug is the superficial gas velocity. The interfacial area and gas voidage fraction are related by

$$d_{32} = \frac{6\varepsilon}{a} \qquad 2.13$$

for spherical bubbles, where d_{32} is a Sauter mean diameter. The important feature of equations 2.9 and 2.10 is that both the bubble size and specific interfacial area depend on the power input per unit volume. Clearly then the rate of mass transfer also depends on Pg / V, so that it is a requirement of any gas-liquid impeller that the gassed power is almost independent of the gas flow rate. Then, the expression for the voidage fraction becomes (using equations 2.11 – 2.13)

$$\varepsilon = \left(\frac{U_g \varepsilon}{V}\right)^{0.5} + 2.16\omega 10^{-4} \left(\frac{\rho_L^{0.2} \left(\frac{P_g}{V}\right)^{0.4}}{\sigma^{0.6}} \right) \left(\frac{U_g}{V}\right)^{0.5} \quad 2.14$$

Calderbank's method is only approximate since it is well known that the power input to the tank is not dissipated uniformly (Laufhutte & Mersmann, 1985); more energy is dissipated in the vicinity of the impeller than in the bulk circulation. Consequently there is a distribution of bubble sizes and voidage fractions throughout the vessel.

CHAPTER 3

MATHEMATICAL MODELLING

3.1 Overview

This chapter gives a description about modeling the aerated stirred tanks and the mathematical modeling of CFD approach. In modeling an aerated stirred tank, Gambit 2.4.6 software was used to determine the model base on the scale and meshing process. The data then has been exported in Fluent 6.3.26 software to processing and determine the correlation. This chapter also will gives description about aerated stirred tank modelling, the turbulence model and the CFD approach for aerated stirred tank. About aerated stirred tank modeling, the scale and geometry for modeling will be showed.

3.2 Introduction

3.2.1 Gas-Liquid Stirred Vessel modeling

On the computational side, most of the simulations of gas–liquid stirred vessels have been carried out under simplified assumptions and, due to the lack in experimental data, strict evaluation of prediction accuracy has not been frequently performed.

Deen *et al*. (2002a) have compared radial and axial gas and liquid velocity profiles measured with the results of Eulerian–Eulerian simulations performed with the CFX-4 code, using the Sliding Grid approach and the k–1 turbulence model. In the simulations, both bubble diameter and gas-liquid dispersion level were fixed. Discrepancies were found between the CFD axial velocity profiles as well as between the observed and calculated gas cavities behind the Rushton turbine blades. A similar modeling approach was adopted by Khopkar *et al*. (2003) for the simulation of a gas–liquid stirred tank equipped with a pitched blade turbine. Lane *et al*. (2002, 2004) adopted the multi fluid model implemented in the CFX-4 code and coalescence and breakage correlations for the simulation of a gas-liquid stirred vessel, for which bubble distribution profiles were available. With their approach, the prediction of the two-phase flow field, bubble size distribution and gas holdup was possible, but full agreement with the experiments was difficult to achieve. Moreover, many adjustable parameters were introduced in the models. A more fundamental approach was pursued by Venneker *et al*. (2002), who adopted a strongly simplified two-dimensional description of the flow field and turned their attention to the prediction of the bubble size distribution by means of population balance equations with coalescence and breakage source terms. Other works on the simulation of gas–liquid stirred vessels were performed (e.g., Bakker and Van den Akker, 1994; Morud and Hjertager, 1996), but they were limited to 2-D or based on black-box methods for the impeller description; it is, therefore, difficult to establish whether the rather unsatisfactory results obtained are to be attributed to the two-phase flow modelling or to the failure in the continuous phase flow field prediction, that has a major influence on the gas phase dispersion. In other papers, limited quantitative comparison with experiments has been provided (Ranade and Deshpande, 1999; Khopkar *et al*. (2006) and only qualitative conclusions can been drawn about the quality of the modelling approaches. Recently, Khopkar and Ranade (2006) and Scargiali *et al*. (2007) have shown that good quantitative prediction of the gas hold-up distribution can be obtained using fully predictive simulations based on the multi fluid model. Overall, the CFD simulations of gas liquid stirred vessels performed so far have mainly been based on Eulerian models for the two phases and great attention has been devoted to the identification of the most appropriate interaction terms in the momentum equations and, in particular, of the bubble drag law correlation. Nevertheless, more computational work and more extensive and quantitative